crystals

MDPI

Article

Corrosion Inhibition of PAAS/ZnO Complex Additive in Alkaline Al-Air Battery with SLM-Manufactured Anode

Guangpan Peng, Yuankun Geng, Chenhao Niu, Hanqian Yang, Weipeng Duan * and Shu Cao *

School of Mechanical Engineering, Wuxi Institute of Technology, Wuxi 214121, China
* Correspondence: duanweipeng@wxit.edu.cn (W.D.); caoshumse@jiangnan.edu.cn (S.C.)

Abstract: In order to improve the electrochemical activity and discharge performance of aluminum–air batteries and to reduce self-corrosion of the anode, an SLM-manufactured aluminum alloy was employed as the anode of the Al-air battery, and the influence of PAAS and ZnO inhibitors taken separately or together on the self-corrosion rate and discharge performance of the Al-air battery in a 4 M NaOH solution were investigated. The experimental result indicated that the effect of a composite corrosion inhibitor was stronger than that of a single corrosion inhibitor. The addition of the compound inhibitor not only promoted the activation of the anode but also formed a more stable composite protective film on the surface of the anode, which effectively slowed down the self-corrosion and improved the utilization rate of the anode. In NaOH/PAAS/ZnO electrolytes, the dissolution of the Al6061 alloy was mainly controlled by the diffusion of the electric charge in the corrosion products or the zinc salt deposition layer. Meanwhile, for the Al-air battery, the discharge voltage, specific capacity, and specific energy increased by 21.74%, 26.72%, and 54.20%, respectively. In addition, the inhibition mechanism of the composite corrosion inhibitor was also expounded. The excellent discharge performance was due to the addition of the composite corrosion inhibitor, which promoted the charge transfer of the anode reaction, improved the anode's activity, and promoted the uniform corrosion of the anode. This study provides ideas for the application of aluminum–air batteries in the field of new energy.

Keywords: Al-air battery; NaOH/PAAS/ZnO; corrosion inhibitor; complex additive; discharge performance

Citation: Peng, G.; Geng, Y.; Niu, C.; Yang, H.; Duan, W.; Cao, S. Corrosion Inhibition of PAAS/ZnO Complex Additive in Alkaline Al-Air Battery with SLM-Manufactured Anode. *Crystals* **2024**, *14*, 1002. https://doi.org/10.3390/cryst14111002

Academic Editor: Yutaka Moritomo

Received: 1 November 2024
Revised: 15 November 2024
Accepted: 16 November 2024
Published: 19 November 2024

1. Introduction

In recent years, with the significant emissions of greenhouse gases and the continuous consumption of fossil fuels, the development and utilization of new energy has attracted widespread attention [1,2]. According to the requirements of sustainable development strategies, it is imperative to utilize the existing metal resources on Earth and develop low-cost, high safety, high energy density, and competitive chemical power systems [3,4].

The aluminum–air battery is a type of semi-fuel power battery with broad application prospects in fields such as new energy vehicles and unmanned aerial vehicles. Aluminum is lightweight, safe, and has good usability [5,6]. It can achieve high energy density storage through three electron transfers, making it an ideal choice for implementing metal–air battery systems and has great potential for future development [7,8]. However, the commercialization of aluminum–air batteries still faces many challenges. The hydrogen evolution reaction of aluminum anodes in alkaline solutions leads to severe self-corrosion of the battery, which can reduce the anode utilization rate of the battery [9]. Improving the corrosion resistance of the anode may also reduce its electrochemical activity, leading to a decrease in discharge voltage. The above issues seriously restrict the development and application of aluminum–air batteries [10,11].

Various approaches have been proposed by researchers to tackle these issues, and one of the most effective and common methods is electrolyte modification. Up until now, inorganic corrosion inhibitors, including zinc oxide (ZnO), have attracted more and more attention because they not only activate the surface passivation layer but they also form a protective film on the Al anode in order to inhibit self-corrosion without losing anode activity [12–18]. However, due to the uneven deposition of the protective film, the improvement in the corrosion inhibition efficiency of the inorganic corrosion inhibitor is limited [19–22]. Research shows that inorganic and organic mixed corrosion inhibitors demonstrate better inhibition, which is attributed to their synergistic effects [23–28]. To reduce the self-corrosion rate of the Al anode in an alkaline solution, Gelman et al. explored the possibility of using hybrid organic/inorganic inhibitors based on polyethylene glycol diacid (PEG diacid) and ZnO [29]. The results showed that the hybrid solution of PEG diacid and ZnO could provide substantial corrosion protection for the Al anode, and its corrosion rate was reduced by more than one order of magnitude. A hybrid corrosion inhibitor combining acrylamide (AM) and ZnO was created by Cheng et al. to suppress the self-corrosion of the aluminum anode and strengthen the discharge performance of an alkaline battery [30]. It turns out that the amide group of AM is adsorbed on the surface of Al and ZnO, and AM enables ZnO to easily aggregate into a layer in close contact with the anode, effectively inhibiting self-corrosion. Jiang et al. constructed three kinds of novel inorganic/organic hybrid corrosion inhibitors (ZnO + acetic acid, citric acid, and EDTA, respectively) and demonstrated that the formation of a dense and uniform zinc film on the Al anode was greatly boosted by organic acid [31]. Li et al. investigated the synergistic effect of ZnO and 8-aminoquinoline (8-AQ) in an alkaline electrolyte for an al-air battery and discovered the compound protective film formed on the aluminum surface delays the release of hydrogen and can effectively improve the discharge performance of the aluminum anode [32].

The above research shows that adding organic inhibitors to the ZnO-containing alkaline electrolyte can decrease the self-corrosion of the aluminum anode. However, in an ongoing study, due to the small number of functional groups in organic inhibitors, the interaction with Al is relatively weak, and the protective effect on the ZnO deposition film is limited [33–36]. Therefore, looking for a corrosion inhibitor with a large number of polar groups is expected to further improve the discharge performance of an Al-Air battery. Sodium polyacrylate (PAAS), an organic solvent with a large number of negatively charged hydrophilic groups such as -COOH and -C=O, can increase the adhesion between the deposited zinc layer and the aluminum surface, promote the formation of a more stable protective layer, and improve the discharge performance of the anode [37–39]. The current literature shows that PAAS has been extensively studied as an electrolyte additive for Zn-air batteries [40–42]; however, few reports focus on its application in alkaline Al-air batteries.

Based on the above analysis, we innovatively introduced PAAS into alkaline electrolytes containing ZnO to investigate the effects of organic and inorganic compound inhibitors on the electrochemical behavior and discharge performance of anodes in a 4 M NaOH solution. We also evaluated the applicability of PAAS and ZnO as composite inhibitors for alkaline aluminum–air batteries to reduce anode self-corrosion, thereby improving their electrochemical activity and discharge performance.

2. Experimental

2.1. Materials

The 6061 Al alloy (Al6061) from Avimetal Powder Metallurgy Technology Co., Ltd., Beijing, China was used as an anode material for its lower hydrogen evolution rate, higher electrochemical properties, and better battery performance [43,44]. The Al6061 anode was prepared using SLM technology, as stated in our previous research [45]. The air cathode (with MnO_2 as the catalyst) was purchased from APS B&D Industrial (Wuxi) Co., Ltd., Wuxi, China, and Changsha Spring New Energy Technology Co., Ltd., Changsha, China, respectively. Sodium hydroxide (NaOH), zinc oxide (ZnO), sodium polyacrylate (PAAS), chromium trioxide (CrO_3), and phosphoric acid (H_3PO_4) were all provided by Sinopharm Chemical Reagent Co., Ltd., Shanghai, China. The electrolyte system in this paper is as follows: 4 M NaOH, 4 M NaOH + 8 g/L ZnO, 4 M NaOH + 2 g/L PAAS, 4 M NaOH + 8 g/L ZnO + 2 g/L PAAS. The specification of materials can be found in Table 1.

Table 1. Specification of materials.

No.	Materials	Specification
1	Al6061	15~53 µm, powder
2	Cathode	commercial
3	NaOH	99%
4	ZnO	99.999%, ≤45 µm, powder
5	PAAS	average Mw 2100
6	CrO_3	98%
7	H_3PO_4	≥85 wt.% in H_2O

2.2. Self-Corrosion Test

All the Al6061 anode samples were cut into specimens with dimensions of 10 mm × 10 mm × 10 mm, then polished by metallographic and silicon carbide waterproof abrasive papers (grades ranged from 400, 800, 1200, to 2000) and ultrasonically cleaned in ethanol solution for 30 min before testing. The polished samples were immersed in four kinds of electrolytes for 60 min each and taken out every 10 min, removed, and then the corrosion products were placed in the mixed solution of 2% CrO_3 and 5% H_3PO_4 at 80 °C for 5 min. A precision electronic balance (XS205-DU, Mettler Toledo, Greifensee, Switzerland) with an accuracy of 0.001 mg was used to calculate the weight loss (Δm) and self-corrosion rate according to Equation (1) [46]:

$$V_\alpha = \frac{\Delta m}{s \cdot t} \tag{1}$$

where V_α is the self-corrosion rate, g/(cm^2·h); Δm is the mass loss before and after corrosion, g; s is the soaking area, cm^2; t is the soaking time, min.

2.3. Electrochemical Measurement

The samples were polished following the method described above and then sealed with insulation and epoxy resin, except for one working surface with an area of 10 mm × 10 mm. The electrochemical tests were carried out by the CHI750E electrochemical workstation (Shanghai Chenhua Instrument Co., Ltd., Shanghai, China). During the test, Al6061 samples were used as the working electrode, and Pt sheets and Hg/HgO were used as the counter electrode and reference electrode, respectively. The open circuit potential (OCP) was measured first until it reached a steady state, and then electrochemical impedance spectroscopy (EIS) was performed. The frequency of the EIS test ranged from 10^5 Hz to 10^{-1} Hz with an amplitude of 5 mV. Finally, the potentiodynamic polarization test was measured at a 1 mV/s scanning rate. Zsimpwin software (version 3.10) was used for data analysis. The schematic of the equipment is shown in Figure 1 (the red circle represents the three electrode system).

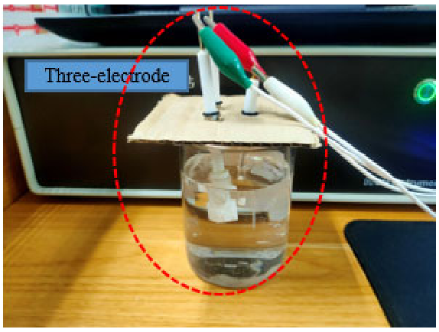

Figure 1. Schematic of the electrochemical testing equipment.

2.4. Discharge Experiment

The polished anode was an Al6061 sample with a working area of 10 mm × 10 mm, while the cathode was a gas diffusion layer with a MnO_2 catalytic active layer with an effective area of 40 mm × 40 mm. The electrolyte solution was 4 M NaOH and its composite inhibitor. The discharge performance of an alkaline air battery was investigated by a constant current discharge at current densities of 10 mA/cm^2 for 3 h utilizing the LAND battery testing system (CT3001AU, Wuhan LAND Electronic Co., Ltd., Wuhan, China). After the experiment, Al6061 samples were immersed in the mixed solution of 2% CrO_3 and 5% H_3PO_4 at 80 °C for 5 min to remove the discharge products on the anode surface. The mass loss of the sample before and after discharge was recorded as Δm, and the anode utilization rate, capacity density, and energy density were also calculated according to Equations (2)–(4), respectively [47,48]:

$$\eta = \frac{100\mathrm{I}\cdot \mathrm{t}}{\Delta \mathrm{m}\cdot \mathrm{F}} \tag{2}$$

$$\mathrm{Q} = \frac{\mathrm{Ih}}{\Delta \mathrm{m}} \tag{3}$$

$$\mathrm{w} = \frac{\mathrm{UIh}}{\Delta \mathrm{m}} \tag{4}$$

where η is the anode utilization rate, %; Q is the capacity density, mAh/g; W is the energy density, wAh/g; Δm is the mass loss of the sample before and after discharge, g; F is the Faraday constant, 96,485 C/mol; h is the discharge time (h); U is the discharge voltage, V. The schematic of the equipment is shown in Figure 2.

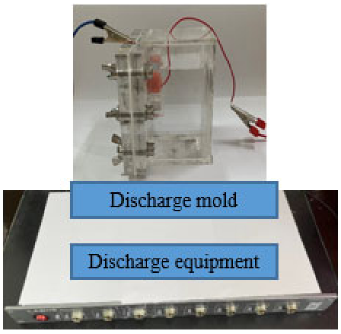

Figure 2. Schematic of the discharge testing equipment.

X-ray diffraction (XRD; Bruker D8 Advance, Karlsruhe, Germany), scanning electron microscopy, and energy dispersive spectroscopy (SEM and EDS; Sigma 300, Hitachi, Chiyoda City, Japan) were also applied to observe and analyze the surface morphology and composition, as shown in Figure 3. To ensure the accuracy of test results, all experiments were measured three times, and the average value was taken as the data in this work.

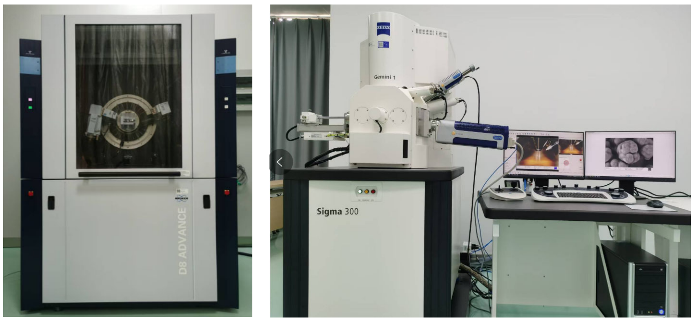

(**a**) XRD equipment (**b**) SEM equipment

Figure 3. Schematic of XRD and SEM equipment.

3. Results and Discussion

3.1. Self-Corrosion Behavior

The mass loss of the Al6061 anode in different electrolytes is shown in Figure 4 and Table 2, the relationship between mass loss and time is deduced. The results show that the mass loss is a linear function of time. Slope k represents the self-corrosion rate of the Al6061 anode (where higher k values indicate higher self-corrosion rates). The significant difference in k values confirm that the electrolyte has an appreciable effect on the self-corrosion rate of the Al anode. In addition, the self-corrosion rate and corrosion inhibitor efficiency of the Al6061 anode and electrolytes are also listed. As shown, the self-corrosion rate of the Al6061 anode is extremely high in the 4 M NaOH electrolyte, the passive film is eliminated in the alkaline solution, and more OH^- reacts with Al, causing the increase in the self-corrosion rate. With the addition of ZnO and PAAS, the self-corrosion rate of the Al6061 anode decreases by 10.21% and 40.07%, respectively, indicating that ZnO and PAAS can inhibit the self-corrosion of the anode. Perhaps more intriguingly, when ZnO and PAAS are added simultaneously, the slope value of the Al6061 anode decreases from 0.4976 $g/cm^2{\cdot}h$ to 0.2723 $g/cm^2{\cdot}h$, and the corrosion inhibition efficiency reaches 45.28%. It is mainly because the adsorption of PAAS increases the adhesion between the deposited zinc layer and the Al surface, thus reducing the self-corrosion. From the above analysis, it is shown that the suppressive effect of self-corrosion may be relatively weak when ZnO and PAAS act separately. In comparison, when used in combination, an obvious promotion is achieved. Therefore, using ZnO and PAAS simultaneously is the most promising approach for reducing the self-corrosion of the Al6061 anode.

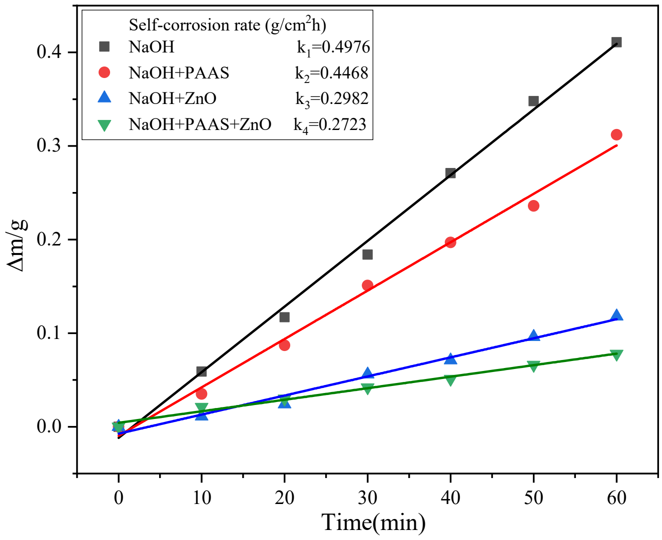

Figure 4. Self-corrosion behavior of the Al6061 anode in different electrolyte systems.

Table 2. Self-corrosion rate of aluminum alloy in different electrolyte systems.

No.	Electrolyte	Self-Corrosion Rate ($g/cm^2{\cdot}h$)
1	NaOH	0.4976 ± 0.037
2	NaOH + PAAS	0.4468 ± 0.039
3	NaOH + ZnO	0.2982 ± 0.043
4	NaOH + ZnO + PAAS	0.2723 ± 0.040

3.2. Electrochemical Properties

The open circuit potential (OCP) curves of the Al6061 anode in different electrolytes are displayed in Figure 5. It can be seen that all curves show a similar tendency toward variation. OCP is basically stable throughout the process, which is attributed to the adsorption of an Al_2O_3 film or $Al(OH)_3$ on the alloy surface produced by an anodic dissolution reaction. In addition, it can be seen that the OCP value of each system is significantly different, which indicates that the added inhibitor has an important impact on the electrochemical performance of Al6061. When inhibitors are added, the OCP shifts significantly negatively. Compared with the electrolyte without inhibitors (OCP is −1.39 V), the OCP shifts by 6.47% and 10.07% after adding PAAS and ZnO, respectively. This is because the cathodic reaction (hydrogen evolution self-corrosion) is inhibited and the excessive electrons released by the anodic reaction accumulate, resulting in a more negative potential. Wang et al. studied the effect of cerium nitrate on the OCP of an aluminum alloy in an alkaline electrolyte, and reached the same conclusion [49]. They believed that the negative shift in OCP was due to the inhibition of cathodic corrosion by cerium nitrate. At the same time, it can be seen that the NaOH + PAAS + ZnO electrolyte represents the most negative OCP (−1.62 V), which is also due to the protective layer formed by PAAS adsorption on the Al661 anode surface, making the zinc layer more stable and dense.

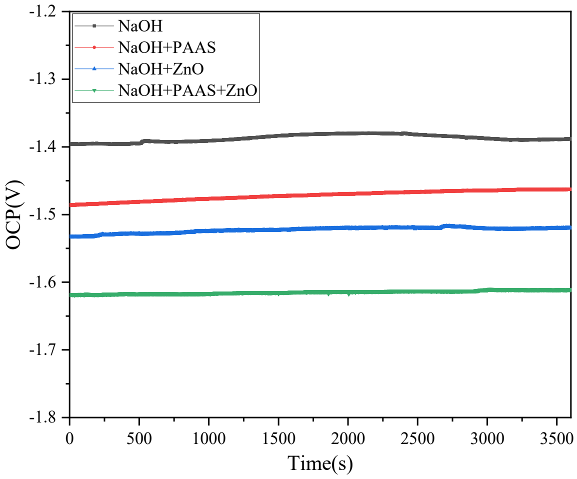

Figure 5. OCP of the Al6061 anode in different electrolyte systems.

The electrochemical dissolution behavior of the Al6061 electrode is analyzed by the potentiodynamic polarization curve, as shown in Figure 6. Electrochemical polarization parameters, including corrosion potential (Ecorr, V), corrosion current density (Jcorr, A/cm^2), and polarization resistance (Rp, $\Omega \cdot cm^2$) are also listed in Table 3.

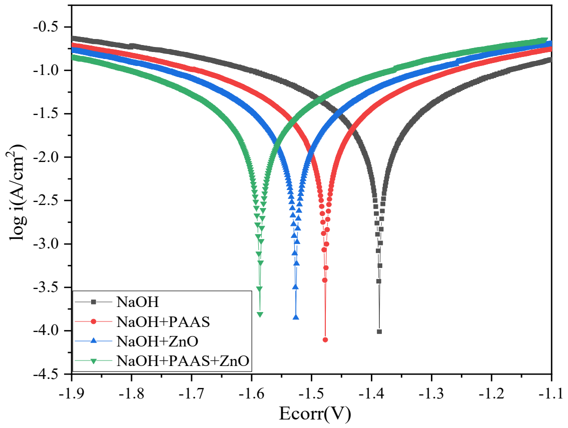

Figure 6. Polarization curve of Al6061 anode in different electrolyte systems.

Ecorr reflects the electrochemical activity of anodic dissolution. Due to the negative difference effect, the self-corrosion of the Al6061 anode during polarization is higher than that before polarization. Therefore, the more negative the corrosion potential, the higher the electrochemical activity of the anode, which relatively weakens the impact of self-corrosion on the discharge performance during the discharge process. Jcorr represents the self-corrosion rate; the higher the Jcorr, the faster the self-corrosion rate, and the worse the corrosion resistance. In the NaOH solution, the anodic polarization curve shows that the current increases monotonously with the potential and finally reaches the current limiting platform. This is because the anodic reaction process begins with an active dissolution stage, then undergoes a diffusion control stage, and finally reaches the equilibrium state. The reactions occurring on the anode are shown in Formulas (5) and (6), while the cathodic reaction is a coupling process of oxygen dissolution and hydrogen evolution, as shown in Formulas (7) and (8).

$$\mathrm{Al} + 3\mathrm{OH}^- \rightarrow \mathrm{Al(OH)_3} \downarrow + 3\mathrm{e}^- \tag{5}$$

$$\mathrm{Al(OH)_3} + \mathrm{OH}^- \rightarrow \mathrm{Al(OH)_4}^- \tag{6}$$

$$\mathrm{O_2} + 2\mathrm{H_2O} + 4\mathrm{e}^- \rightarrow 4\mathrm{OH}^- \tag{7}$$

$$2\mathrm{H_2O} + 2\mathrm{e}^- \rightarrow 2\mathrm{OH}^- + \mathrm{H_2} \tag{8}$$

Table 3. Polarization parameters of Al-air battery anode in different electrolyte systems.

Electrolytes	Electrochemical Parameters		
	Ecorr (V)	Jcorr (A/cm^2)	Rp (Ω·cm^2)
NaOH	−1.39	4.882×10^{-2}	2.4
NaOH + PAAS	−1.48	3.726×10^{-2}	3.5
NaOH + ZnO	−1.53	2.529×10^{-2}	3.9
NaOH + ZnO + PAAS	−1.59	1.587×10^{-2}	4.8

From the polarization curve and its parameters, it can be seen that the corrosion potential of the Al6061 anode is close to its OCP. After adding corrosion inhibitors, the Ecorr becomes significantly negative, and the NaOH + PAAS + ZnO solution has the most negative Ecorr and the smallest Jcorr, which shows that the addition of compound inhibitors not only improves the electrochemical activity of the Al6061 anode but also reduces its self-corrosion rate. As a phase-forming inhibitor, ZnO forms a Zn layer on the surface of the anode, and the deposited zinc is dissolved in an alkaline solution to form ZnO or zinc salts, the chemical reaction shown in Formulas (9) and (10).

$$\mathrm{ZnO} + \mathrm{H_2O} + 2\mathrm{OH}^- = \mathrm{Zn(OH)_4}^{2-} \tag{9}$$

$$3\mathrm{Zn(OH)_4}^{2-} + 2\mathrm{Al} = 3\mathrm{Zn} + 2\mathrm{Al(OH)_4}^- + 4\mathrm{OH}^- \tag{10}$$

The deposition of these reaction products leads to the reduction in the cathode current. Zinc passivation film has a higher hydrogen evolution overpotential than Al and plays an important role in inhibiting hydrogen evolution. However, the zinc layer deposited in an alkaline solution is unstable and easy to break. The directional arrangement of negatively charged hydrophilic groups in PAAS increases the adhesion between the deposited zinc layer and the aluminum surface, forming a more stable zinc layer, and improves the anode discharge performance. In addition, -COOH takes part in the deprotonation reaction to adsorb Al^{3+}, inhibits the adsorption of corrosion products on the anode surface, and maintains the anode's activity.

In order to further analyze the electrochemical characteristics of the Al6061 anode, electrochemical impedance spectroscopy (EIS) is also applied to characterize the anode. The obtained Nyquist plots of the fitted equivalent circuit and the corresponding fitting parameters are shown in Figures 7 and 8, and Table 4, respectively. As shown in Figure 5, Rs is the solution resistance, Rt is the charge transfer resistance (Al-Al^+), R_2 is the charge transfer resistance (Al^+-Al^{3+}), Zw represents the Warburg impedance caused by the deposited zinc layer or the diffusion of corrosion products, and CPE_1 and CPE_2 are the constant phase angles of the double-layer capacitance. As can be seen in Figure 5, the EIS of the Al6061 alloy in the NaOH and NaOH + PAAS solutions consists of two capacitive reactance arcs, that is, high-frequency and low-frequency capacitive reactance arcs, indicating that the addition of PAAS does not interfere with the anodic chemical reaction process. The high-frequency capacitive reactance arc is caused by the charge transfer of the electrochemical reaction (Al-Al^{3+}) on the alloy surface, and the low-frequency capacitive arc is caused by the attachment of passivation film or corrosion products on the alloy surface. The size of the capacitive reactance arc, as shown in reaction Formula (5), reflects the charge transfer rate. In addition, it can be seen that the high-frequency capacitance arc in the NaOH + PAAS solution is smaller than that in the NaOH solution. This is because the addition of PAAS increases the viscosity of the solution and reduces the conductivity and charge transfer rate, but the impact is small. But, specifically, the degree of influence is quite limited. The low-frequency capacitive arc in the NaOH + PAAS solution is larger than that in the NaOH solution, which is caused by the adsorption of PAAS. Obviously, the EIS of the Al6061 alloy in NaOH + ZnO and NaOH + PAAS + ZnO is significantly different from the previous one. As shown in Figure 5, the EIS consists of a high-frequency capacitive reactance arc and a low-frequency 45° oblique line. The high-frequency capacitive arc of EIS in the NaOH + PAAS + ZnO solution is larger than that in the NaOH + ZnO solution, indicating that the addition of PAAS makes the deposited zinc layer more compact and stable and promotes the charge transfer of anodic reactions. The low-frequency 45° oblique line is caused by semi-infinite diffusion and is a typical feature of Warburg impedance. This shows that the electrochemical reaction of Al6061 in NaOH + ZnO and NaOH + PAAS + ZnO electrolytes is controlled by the diffusion of the electric charge in corrosion products or the deposited zinc layer.

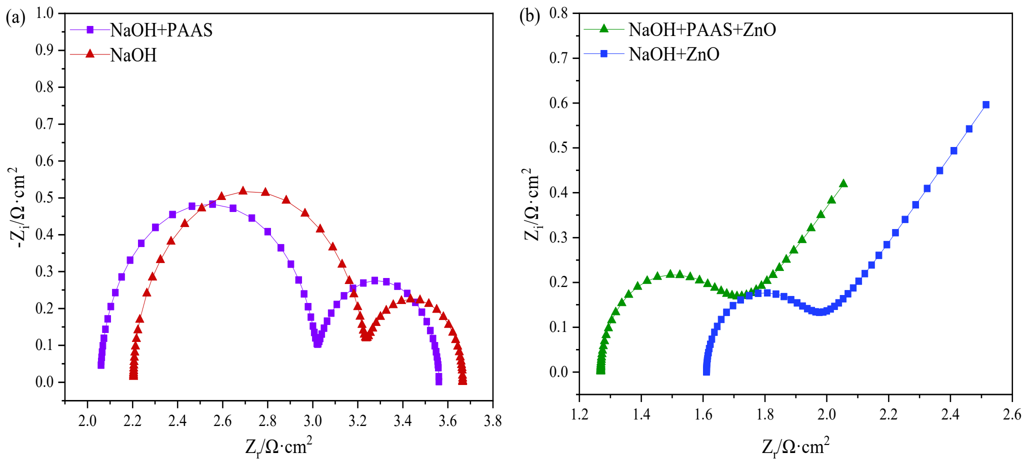

Figure 7. EIS of the Al6061 anode in different electrolyte systems: (**a**) NaOH and NaOH + PAAS; (**b**) NaOH + ZnO and NaOH + PAAS + ZnO.

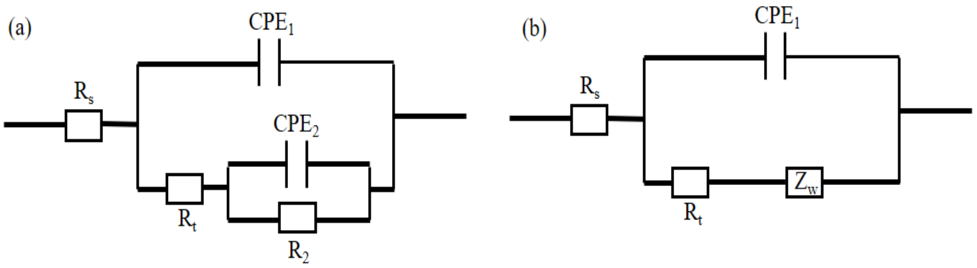

Figure 8. Equivalent circuit of the Al6061 anode in different electrolyte systems: (**a**) NaOH and NaOH + PAAS; (**b**) NaOH + ZnO and NaOH + PAAS + ZnO.

Table 4. EIS parameters of the Al6061 anode in different electrolyte systems.

Electrolytes	**R_s /Ω cm^2**	**CPE$_1$ /F cm^{-2}**	**R_t /Ω cm^2**	**CPE$_2$ /F cm^{-2}**	**R_2 /Ω cm^2**	**Z_w /Ω cm^2**	χ^2
NaOH	2.853	5.156×10^{-5}	0.9878	0.3183	0.6836	/	4.837×10^{-3}
NaOH + PAAS	2.671	2.556×10^{-4}	1.036	0.4265	0.5571	/	5.618×10^{-3}
NaOH + ZnO	1.786	2.716×10^{-3}	0.4831	/	/	0.7523	3.671×10^{-3}
NaOH+ ZnO + PAAS	1.386	3.594×10^{-3}	0.2351	/	/	4.896	4.248×10^{-3}

3.3. Battery Performance

To investigate the discharge characteristics of the Al-air battery across various electrolyte systems, a controlled current discharge experiment is conducted, and the discharge curve is depicted in Figure 9. Notably, the discharge profiles of the Al6061 anode in different electrolyte systems exhibits a consistent trend: an initial rapid voltage decline followed by a gradual stabilization. The steep voltage drop observed initially is attributed to the electrode transitioning from a polarized state to an activated state. As the Al6061 anode continues to discharge, the voltage curve flattens out. In the NaOH + ZnO electrolyte system, the voltage curve displays a fluctuation pattern. This fluctuation is due to the cyclic adhesion and detachment of the zinc salt deposition layer on the surface of the Al6061 anode. Conversely, in the NaOH + PAAS + ZnO electrolyte system, the discharge voltage is not only the highest but also the most stable. This suggests that the incorporation of PAAS effectively safeguards the zinc salt deposition layer, preventing it from covering the active discharge areas and thus significantly enhancing battery performance.

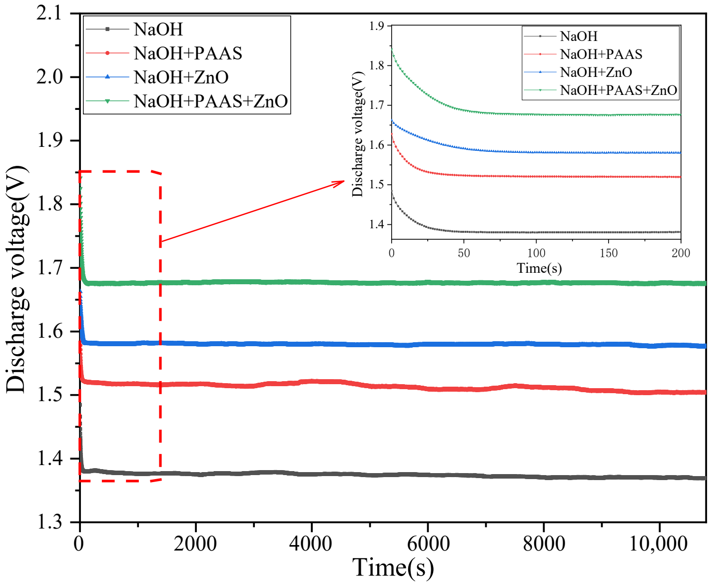

Figure 9. Discharge curve of the Al-air battery in different electrolyte systems.

To analyze the variations in discharge characteristics across different electrolytes, a comparative assessment and calculation of the anode utilization, specific capacity, and specific energy of the Al6061 anode is conducted, with the results presented in Figure 10. The data reveal that, in a NaOH electrolyte, the anode utilization stands at 50.6%. Upon the addition of PAAS and ZnO, the anode utilization rate experiences an increase of 11.86% and 16.60%, respectively. Following a similar upward trend as the anode utilization, the specific capacity rises by 11.74% and 16.71%, while the specific energy sees an enhancement of 21.75% and 34.89% after incorporating PAAS and ZnO. These findings suggest that the inclusion of PAAS and ZnO can effectively elevate the discharge performance of an Al-Air battery. More strikingly, in the NaOH + PAAS + ZnO electrolyte system, the anode utilization, specific capacity, and specific energy exhibit substantial increases of 26.68%, 26.72%, and 54.20%, respectively. This underscores the synergistic effect of PAAS and ZnO when used together, significantly enhancing the discharge capabilities of the battery.

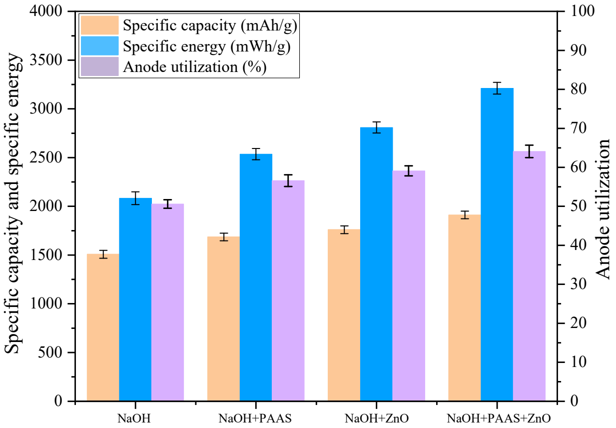

Figure 10. Battery performance parameters of Al6061 anode in different porous electrolytes.

In order to further analyze the surface morphology and discharge products, SEM, EDS, and XRD are also manipulated. Figure 11 shows the surface SEM images of the Al6061 anode before and after discharge. The element composition of different areas and the EDS spectra of points A to F are shown in Figure 12. It can be seen in Figure 11a that the Al6061 anode surface shows serious lamellar corrosion in the NaOH solution without a corrosion inhibitor. When PAAS is added to the electrolyte, it can be observed in Figure 11b that the anode surface is covered with an uneven film, with regions A, B, and C containing more O elements and a small amount of C elements; this is due to the formation of the corrosion product $Al(OH)_{ads}$ and the adsorption of PAAS. As shown in Figure 11c, the surface shows cracks and rough surface morphology, which are due to the zinc salt deposition layer attached to the Al6061 alloy surface. When PAAS and ZnO are added to the electrolyte at the same time, a more uniform protective film is formed on the surface, as shown in Figure 11d. There are C and Zn elements at the D, E, and F positions, which means that a composite film of ZnO and PAAS is formed on the surface of the alloy. The stable protective film formed can inhibit the hydrogen evolution of the anode and reduce the self-corrosion rate. During the discharge process, Al^{3+} ions can still enter the electrolyte through the micro-pores in the membrane. Therefore, the Al6061 anode still retains positive electrochemical activity.

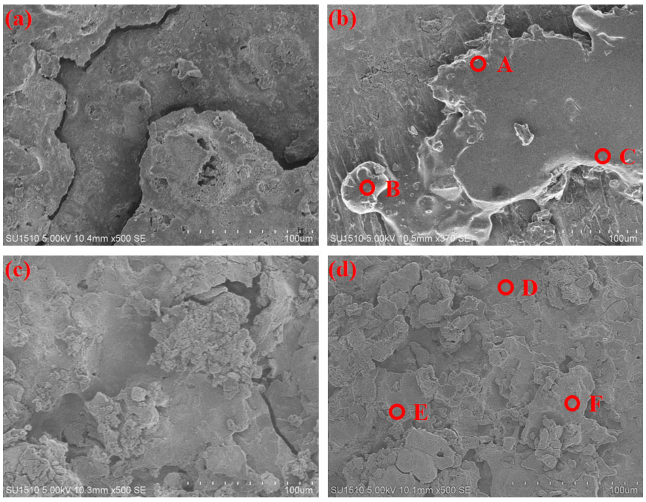

Figure 11. Surface morphology of the Al6061 anode after discharge in different electrolyte systems: (**a**) NaOH; (**b**) NaOH + PAAS; (**c**) NaOH + ZnO; (**d**) NaOH + PAAS + ZnO.

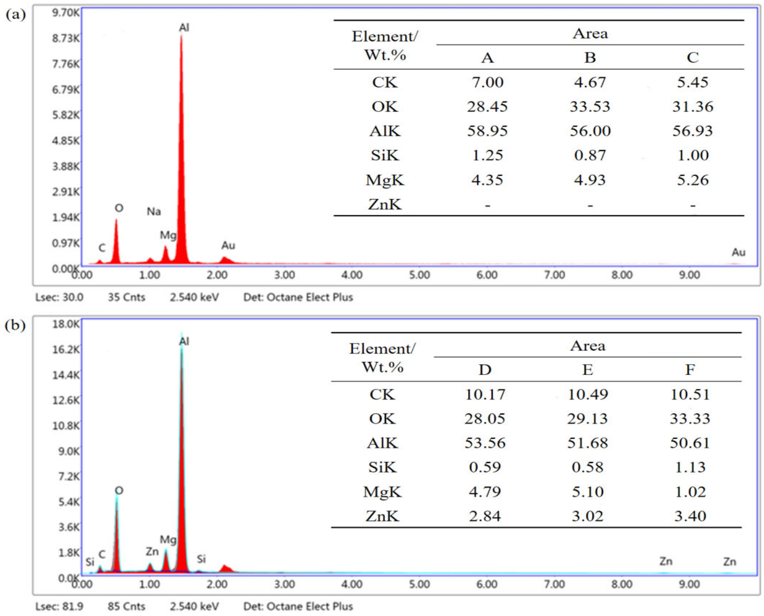

Element/ Wt.%	Area		
	A	B	C
CK	7.00	4.67	5.45
OK	28.45	33.53	31.36
AlK	58.95	56.00	56.93
SiK	1.25	0.87	1.00
MgK	4.35	4.93	5.26
ZnK	-	-	-

Element/ Wt.%	Area		
	D	E	F
CK	10.17	10.49	10.51
OK	28.05	29.13	33.33
AlK	53.56	51.68	50.61
SiK	0.59	0.58	1.13
MgK	4.79	5.10	1.02
ZnK	2.84	3.02	3.40

Figure 12. Element composition of the corresponding area in Figure 11 and EDS atlas of point A to point F: (**a**) point A, B and C; (**b**) point D, E and F.

The XRD pattern of surface corrosion products after discharge is shown in Figure 13. As shown in Figure 13a, in the NaOH + PAAS electrolyte, the corrosion products are mainly $Al(OH)_{ads}$, which exist in the form of $Al_2O_3{\cdot}H_2O$ after separating from the solution. It shows that in Figure 13b the corrosion products in the NaOH + PAAS + ZnO solution are mainly $Al_2O_3{\cdot}H_2O$, Zn, and $Zn(OH)_2$, which confirms that ZnO reacts in the solution, as shown in Formulas (9) and (10), to form a zinc salt deposit. However, due to the cleaning and drying treatment, the corrosion product layer becomes thinner, and the peak value of Zn and $Zn(OH)_2$ is smaller. In addition, PAAS does not participate in electrode reactions but only adsorbs on the surface of the Al6061 anode by electrostatic action, which is an adsorptive corrosion inhibitor.

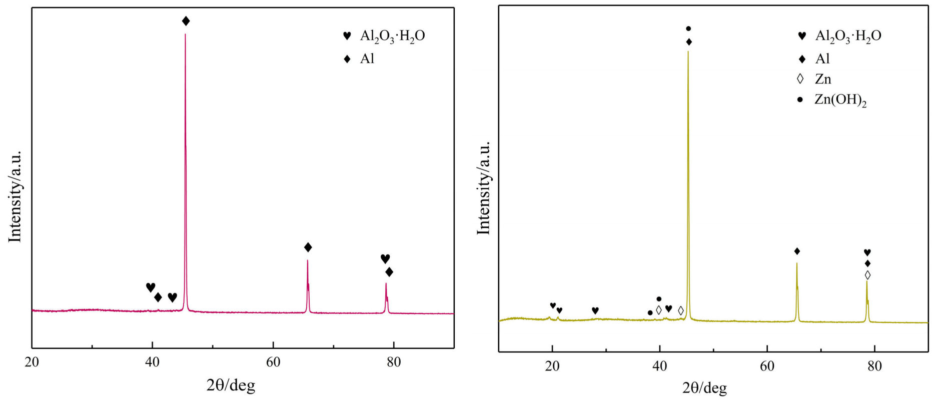

(**a**) NaOH + PAAS electrolyte (**b**) NaOH + PAAS + ZnO electrolyte

Figure 13. XRD pattern of surface corrosion products of the Al6061 anode after discharge in different electrolytes.

The inhibition mechanism of the Al6061 anode in different electrolyte systems is shown in Figure 14. ZnO forms a zinc layer protective film on the surface of the alloy, which has a higher hydrogen evolution potential than Al, thus inhibiting the hydrogen evolution self-corrosion of the anode. However, the zinc layer is loose and falls off easily. The negatively charged hydrophilic group of PAAS is adsorbed on the surface of the deposition layer through electrostatic action, forming a similar structure like a "sandwich" with the Al6061 anode, which increases the adhesion between the deposited zinc layer and the surface of anode. Therefore, a more stable phase-forming zinc layer is formed, which reduces the self-corrosion rate and improves the discharge performance of the Al-air battery.

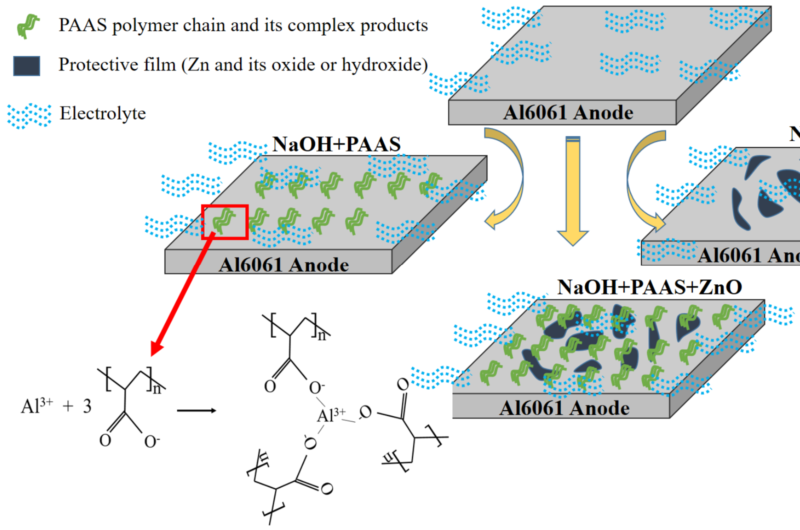

Figure 14. Inhibition mechanism of the Al6061 anode in different electrolyte systems.

4. Conclusions

In this paper, an Al6061 alloy is used as the anode of an Al-air battery, and the effects of PAAS and ZnO inhibitors taken separately or together on the self-corrosion and discharge performances of the Al-air battery in a 4 M NaOH solution are studied. The main conclusions are as follows:

(1) The effect of a PAAS + ZnO compound corrosion inhibitor is stronger than that of a single inhibitor.

(2) A PAAS + ZnO compound corrosion inhibitor reduces the self-corrosion rate of the Al6061 anode and improves the discharge performance of the Al-air battery. The self-corrosion rate decreases from 0.4976 $\text{g/cm}^2\cdot\text{h}$ to 0.2723 $\text{g/cm}^2\cdot\text{h}$. Meanwhile, the discharge voltage shifts negatively, and the anode utilization, specific capacity and specific energy increase by 26.68%, 26.72%, and 54.20%, respectively.

(3) ZnO is a phase-forming corrosion inhibitor that mainly inhibits anode self-corrosion through the formation of a zinc layer, whereas PAAS is an adsorptive corrosion inhibitor, and its electrostatic adsorption makes the composite protective film more stable and dense.

(4) In the NaOH + PAAS + ZnO electrolyte, the dissolution of the Al6061 anode is mainly controlled by the diffusion of the electric charge in the corrosion products or the zinc salt deposition layer. The addition of PAAS + ZnO composite corrosion inhibitor promotes the charge transfer of anode reactions, improves the anode activity, and promotes uniform corrosion, thus increasing the discharge performance and making it more stable.

This work focuses on the current research status of Al-air batteries. A composite electrolyte is prepared and tested, which improves its electrochemical activity and discharge performance to a certain extent. However, in alkaline media, the flow reaction and corrosion reaction products of the aluminum anode are both gel-like aluminum hydroxide, which reduces the conductivity of the electrolyte and increases the polarization of the aluminum anode, thereby deteriorating the battery performance. In addition, the electrolyte needs to be able to form a rapid anodic oxidation reaction response mechanism with the aluminum electrode while maintaining an efficient and stable ion transfer. Therefore, there is still insufficient research on how reaction products affect electrolyte conductivity, ion transfer efficiency, and stability, and further optimization of electrolyte composition and ratio is needed.

Author Contributions: Investigation, G.P. and W.D.; software and data curation, Y.G., C.N. and H.Y.; writing—original draft preparation, G.P. and W.D.; resources and writing—review, S.C. All authors have read and agreed to the published version of the manuscript.

Funding: This study was supported by the Qing Lan Project of Jiangsu Province (Funder: Shu Cao) and the Natural Science Research Project of Wuxi Institute of Technology (Funder: Weipeng Duan. No. BT2024-13).

Data Availability Statement: The original contributions presented in this study are included in the article; further inquiries can be directed toward the corresponding authors.

Acknowledgments: This study was supported by the National Center of Supervision and Inspection on Additive Manufacturing Products Quality.

Conflicts of Interest: There are no conflicts of interest to declare.

References

1. Liu, S.; Ban, J.; Shi, H.; Wu, H.; Shao, G.; Cao, G.; Hu, J. Near solution-level conductivity of polyvinyl alcohol based electrolyte and the application for fully compliant Al-air battery. *Chem. Eng. J.* **2022**, *431*, 134283. [CrossRef]
2. Tu, J.; Song, W.; Lei, H.; Yu, Z.; Chen, L.; Wang, M.; Jiao, S. Nonaqueous rechargeable aluminum batteries: Progresses, challenges, and perspectives. *Chem. Rev.* **2021**, *121*, 4903–4961. [CrossRef] [PubMed]
3. Buckingham, R.; Asset, T.; Atanassov, P. Aluminum-air batteries: A review of alloys, electrolytes and design. *J. Power Sources* **2021**, *498*, 229762. [CrossRef]
4. Hassan, M.; Sen, A.; Zaman, T.; Mostari, M. Emergence of graphene as a promising anode material for rechargeable batteries: A review. *Mater. Today Chem.* **2019**, *11*, 225–243. [CrossRef]
5. Chen, Z.; Yu, A.; Drew, H.; Li, H.; Wang, H.; Chen, Z. Highly active and durable core-corona structured bifunctional catalyst for rechargeable metal-air battery application. *Nano Lett.* **2012**, *12*, 1946–1952. [CrossRef]
6. Liu, W.; Liu, P.; Mitlin, D. Review of emerging concepts in SEI analysis and artificial SEI membranes for lithium, sodium, and potassium metal battery anodes. *Adv. Energy Mater.* **2020**, *10*, 2002297. [CrossRef]
7. Gu, B.; Yoon, S.; Park, S.; Byun, S.; Cha, S. A study on the application of metal-air battery to large size uninterruptible power supply with a hybrid system. *JMST Adv.* **2019**, *1*, 181–190. [CrossRef]
8. Levy, N.; Lifshits, S.; Yohanan, E.; Yair, E. Hybrid ionic liquid propylene carbonate-based electrolytes for aluminum-air batteries. *ACS Appl. Energy Mater.* **2020**, *3*, 2585–2592. [CrossRef]
9. Yu, Y.; Chen, M.; Wang, S.; Hill, C.; Joshi, P.; Kuruganti, T.; Hu, A. Laser sintering of printed anodes for Al-air batteries. *J. Electrochem. Soc.* **2018**, *165*, A584–A592. [CrossRef]
10. Hou, C.; Chen, S.; Wang, Z.; Wang, G.; Dong, G. Effect of 6-thioguanine, as an electrolyte additive, on the electrochemical behavior of an Al-air battery. *Mater. Corros.* **2020**, *71*, 1480–1487. [CrossRef]
11. Osório, W.; Freitas, E.; Garcia, A. EIS parameters and cell spacings of an Al-Bi alloy in NaCl solution. *Electrochim. Acta* **2013**, *108*, 781–787. [CrossRef]
12. Liu, Y.; Gao, Z.; Li, Z.; Zhang, J.; Qin, Z.; Wu, Z.; Hu, W.; Tang, Y.; Xu, Y. Inhibiting hydrogen evolution reaction by adjusting electrophilicity of quaternary ammonium salts for aluminum-air battery. *J. Energy Storage* **2024**, *88*, 111537. [CrossRef]
13. Slaughter, G.; Sunday, J.; Stevens, B. Energy conversion from aluminium and phosphate rich solution via ZnO activation of aluminium. *Mater. Chem. Phys.* **2015**, *163*, 245–252. [CrossRef]
14. Prabukumar, C.; Meti, S.; Bhat, U. Enhancing the electrochemical performance of ZnO anode by novel additive of MoS_2-SnO_2 nanocomposite for the zinc alkaline battery application. *J. Mater. Sci. Mater. Electron.* **2022**, *33*, 2534–2549. [CrossRef]
15. Sun, Z.; Lu, H.; Hong, Q.; Liang, F.; Chen, C.; Leng, J. Evaluation of an alkaline electrolyte system for Al-air Battery. *ECS Electrochem. Lett.* **2015**, *4*, A133–A136. [CrossRef]
16. Sun, Y.; Li, Z.; Wu, Y.; Tian, J.; Wang, Y.; Yang, M.; Zhang, G. Formamide-soluble solid-state ZnO as Zn source for synthesizing FeCo-NC with ultrahigh oxygen reduction reaction activity. *Mater. Chem. Front.* **2022**, *6*, 78–85. [CrossRef]
17. Liu, Y.; Sun, Q.; Yang, X.; Liang, J.; Wang, B.; Koo, A.; Li, R.; Li, J.; Sun, X. High-performance and recyclable Al-air coin cells based on Eco-friendly chitosan hydrogel membranes. *ACS Appl. Mater. Interfaces* **2018**, *10*, 19730–19738. [CrossRef]
18. Faegh, E.; Shrestha, S.; Zhao, X.; Mustain, W. In-depth structural understanding of zinc oxide addition to alkaline electrolytes to protect aluminum against corrosion and gassing. *J. Appl. Electrochem.* **2019**, *49*, 895–907. [CrossRef]
19. Ma, J.; Li, W.; Wang, G.; Li, Y.; Ren, F.; Xiong, Y. Influences of L-cysteine/Zinc oxide additive on the electrochemical behavior of pure aluminum in alkaline solution. *J. Electrochem. Soc.* **2018**, *165*, A266–A272. [CrossRef]
20. Liu, Y.; Jiang, H.; Hao, J.; Liu, Y.; Shen, H.; Li, W.; Li, J. Metal-organic framework derived reduced graphene oxide supported $ZnO/ZnCo_2O_4/C$ hollow nanocages as cathode catalysts for Aluminum-O_2 batteries. *ACS Appl. Mater. Interfaces* **2017**, *9*, 31841–31852. [CrossRef]

21. Zhu, C.; Yang, H.; Wu, A.; Zhang, D.; Gao, L.; Lin, T. Modified alkaline electrolyte with 8-hydroxyquinoline and ZnO complex additives to improve Al-air battery. *J. Power Sources* **2019**, *432*, 55–64. [CrossRef]
22. Wang, Y.; Yu, Y.; Wang, J.; Peng, L.; Zuo, Y.; Zuo, C. Novel multifunctional Janus-type membrane on Al anode for corrosion protection. *Adv. Mater. Interfaces* **2021**, *8*, 2100786. [CrossRef]
23. Hwang, B.; Oh, E.; Kim, K. Observation of electrochemical reactions at Zn electrodes in Zn-air secondary batteries. *Electrochim. Acta* **2016**, *216*, 484–489. [CrossRef]
24. Ma, J.; Wen, J.; Gao, J.; Li, Q. Performance of Al-0.5 Mg-0.02 Ga-0.1 Sn-0.5 Mn as anode for Al-air battery. *J. Electrochem. Soc.* **2014**, *161*, A376–A380. [CrossRef]
25. Sun, Z.; Lu, H. Performance of Al-0.5 In as anode for Al-air battery in inhibited alkaline solutions. *J. Electrochem. Soc.* **2015**, *162*, A1617–A1623. [CrossRef]
26. Pino, M.; Chacon, J.; Fatas, E.; Ocan, P. Performance of commercial aluminium alloys as anodes in gelled electrolyte aluminium-air batteries. *J. Power Sources* **2015**, *299*, 195–201. [CrossRef]
27. Liu, J.; Wang, D.; Zhang, D.; Gao, L.; Lin, T. Synergistic effects of carboxymethyl cellulose and ZnO as alkaline electrolyte additives for aluminium anodes with a view towards Al-air batteries. *J. Power Sources* **2016**, *335*, 1–11. [CrossRef]
28. Koç, R.; Özkeçeci, S. The fabrication of exfoliated graphite sheet-based air cathodes and gel electrolyte for metal-air batteries. *Energy Sources Part A Recovery Util. Environ. Eff.* **2019**, *41*, 1779–1789. [CrossRef]
29. Gelman, D.; Lasman, I.; Elfimchev, S.; Starosvetsky, D.; Ein-Eli, Y. Aluminum corrosion mitigation in alkaline electrolytes containing hybrid inorganic/organic inhibitor system for power sources applications. *J. Power Sources* **2015**, *285*, 100–108. [CrossRef]
30. Cheng, H.; Wang, T.; Li, Z.; Guo, C.; Lai, J.; Tian, Z. Anode interfacial layer construction via hybrid inhibitors for high-performance Al-air batteries. *ACS Appl. Mater. Interfaces* **2021**, *13*, 51726–51735. [CrossRef]
31. Jiang, H.; Yu, S.; Li, W.; Yang, Y.; Yang, L.; Zhang, Z. Inhibition effect and mechanism of inorganic-organic hybrid additives on three-dimension porous aluminum foam in alkaline Al-air battery. *J. Power Sources* **2020**, *448*, 227460. [CrossRef]
32. Li, X.; Li, J.; Zhang, L.; Gao, L.; Qu, J.; Lin, T. Synergistic effect of 8-aminoquinoline and ZnO as hybrid additives in alkaline electrolyte for Al-air battery. *J. Mol. Liq.* **2021**, *322*, 114946. [CrossRef]
33. Zhao, S.; Wang, K.; Tang, S.; Liu, X.; Peng, K.; Xiao, Y.; Chen, Y. A new solid-state zinc-air battery for fast charge. *Energy Technol.* **2020**, *8*, 1901229. [CrossRef]
34. Ma, L.; Zhao, Y.; Jie, X.; Zeng, J.; Yang, Q.; Guo, Y.; Huang, Z.; Li, X.; Yu, J.; Zhi, C. A usage scenario independent "Air Chargeable" flexible zinc ion energy storage device. *Adv. Energy Mater.* **2019**, *9*, 1900509. [CrossRef]
35. Zhang, Y.; Chen, Y.; Alfred, M.; Huang, F.; Liao, S.; Chen, D.; Li, D.; Wei, Q. Alkaline sodium polyacrylate-starch hydrogels with tolerance to cold conditions for stretchable zinc-air batteries. *Adv. Mater. Technol.* **2023**, *8*, 2201092. [CrossRef]
36. Cui, M.; Bai, X.; Zhu, J.; Han, C.; Huang, Y.; Kang, L.; Zhi, C.; Li, H. Electrochemically induced $NiCoSe_2$@NiOOH/CoOOH heterostructures as a multifunctional cathode material for flexible hybrid Zn battery. *Energy Storage Mater.* **2021**, *36*, 427–434. [CrossRef]
37. Niu, Y.; Teng, X.; Gong, S.; Xu, M.; Sun, S.; Chen, Z. Engineering two-phase bifunctional oxygen electrocatalysts with tunable and synergetic components for flexible Zn-air batteries. *Nano-Micro Lett.* **2021**, *13*, 126. [CrossRef]
38. Sun, Y.; Fu, C.; Ren, J.; Jiang, M.; Guo, M.; Cheng, R.; Zhang, J.; Sun, B. Highly conductive and reusable electrolyte based on sodium polyacrylate composite for flexible Al-air batteries. *J. Electrochem. Soc.* **2020**, *167*, 080502. [CrossRef]
39. Huang, Z.; Li, X.; Yang, Q.; Ma, L.; Mo, F.; Liang, G.; Wang, D.; Liu, Z.; Li, H.; Zhi, C. Ni_3S_2/Ni nanosheet arrays for high-performance flexible zinc hybrid batteries with evident two-stage charge and discharge processes. *J. Mater. Chem. A* **2019**, *7*, 18915–18924. [CrossRef]
40. Huang, Y.; Li, Z.; Pei, Z.; Liu, Z.; Li, H.; Zhu, M.; Fan, J.; Dai, Q.; Zhang, M.; Dai, L.; et al. Solid-state rechargeable Zn//NiCo and Zn-air batteries with ultralong lifetime and high capacity: The role of a sodium polyacrylate hydrogel electrolyte. *Adv. Energy Mater.* **2018**, *8*, 1802288. [CrossRef]
41. Ma, L.; Chen, S.; Wang, D.; Yang, Q.; Mo, F.; Liang, G.; Li, N.; Zhang, H.; Zapien, J.; Zhi, C. Super-stretchable zinc-air batteries based on an alkaline-tolerant dual-network hydrogel electrolyte. *Adv. Energy Mater.* **2019**, *9*, 1803046. [CrossRef]
42. Chen, S.; Ma, L.; Wu, S.; Wang, Z.; Li, A.; Emmanuel, R.; Zhi, C.; Zapien, J. Uniform virus-like Co-N-Cs electrocatalyst derived from prussian blue analog for stretchable fiber-shaped Zn-air batteries. *Adv. Funct. Mater.* **2020**, *9*, 1908945. [CrossRef]
43. Wang, T.; Zhu, Y.; Li, Y.; Yang, K.; Lu, W.; Peng, K.; Tian, Z. Investigation of commercial aluminum alloys as anode materials for alkaline aluminum-air batteries. *Sustain. Energ. Fuels* **2023**, *7*, 300–309. [CrossRef]
44. Katsoufis, P.; Mylona, V.; Politis, C.; Avgouropoulos, G.; Lianos, P. Study of some basic operation conditions of an Al-air battery using technical grade commercial aluminum. *J. Power Sources* **2020**, *450*, 227624. [CrossRef]
45. Peng, G.; Niu, C.; Geng, Y.; Duan, W.; Cao, S. Multi-objective optimization for the forming quality of a CeO_2/Al6061 alloy as an aluminum-air battery anode manufactured via selective laser melting. *Crystals* **2024**, *14*, 784. [CrossRef]
46. Ren, J.; Ma, J.; Zhang, J.; Fu, C.; Sun, B. Electrochemical performance of pure Al, Al-Sn, Al-Mg and Al-Mg-Sn anodes for Al-air batteries. *J. Alloys Compd.* **2019**, *808*, 151708. [CrossRef]
47. Peng, G.; Huang, J.; Gu, Y.; Song, G. Self-corrosion, electrochemical and discharge behavior of commercial purity Al anode via Mn modification in Al-air battery. *Rare Metals* **2021**, *40*, 3501–3511. [CrossRef]

48. Zhang, H.; Zheng, Y.; Yin, G.; Zou, J.; Wu, Z. The influence of Ga, Sn, or Bi addition on the electrochemical behavior and discharge performance of Al-Zn-In anodes for Al-air batteries. *J. Mater. Sci.* **2021**, *56*, 11011–11026. [CrossRef]
49. Wang, D.; Li, H.; Liu, J.; Zhang, D.; Gao, L.; Tong, L. Evaluation of AA5052 alloy anode in alkaline electrolyte with organic rare-earth complex additives for Aluminum-air batteries. *J. Power Sources* **2015**, *293*, 484–491. [CrossRef]